Int. J. Electrochem. Sci., 17 **(2022)** Article Number: 221223, doi: 10.20964/2022.12.22

International Journal of
ELECTROCHEMICAL
SCIENCE
www.electrochemsci.org

Electrodeposition of NiP/SiC Composite Coating on A105 Steel and Its Corrosion Resistance in Simulated Concrete Pore Solution

Xiaomei Gao

Xi'an Shiyou University, Xi'an, ShanXi, 710065, China
E-mail: gaoxm_syuniv@126.com

Received: 27 September 2022 / *Accepted:* 18 October 2022 / *Published:* 17 November 2022

In the paper, Ni coating, NiP coating and NiP/SiC composite coating were prepared on A105 steel by electrodeposition. The chronoamperometry curves, corrosion resistance, thickness, roughness and surface morphology of different electrodeposited coatings are studied. Nano-SiC particles are positively charged in an aqueous solution, which will migrate to the cathode surface and embed into Ni and NiP alloy coating during electrodeposition to form NiP/SiC composite coating. It is found that the nano-SiC embedded in NiP alloy can increase coating thickness, refine the grains, and greatly reduce the roughness. Compared to Ni coating and NiP coating, the NiP/SiC composite coating possesses the best corrosion resistance with the smallest corrosion current density (7.94 μA/cm^2) and the most positive corrosion potential (-0.417 V).

Keywords: NiP/SiC composite coating; Corrosion resistance; Simulated concrete pore solution; Electrodeposition;

1. INTRODUCTION

Carbon steel is a kind of iron-carbon alloy with a carbon content of 2 %. Carbon steel is widely used in the fields of construction materials, mechanical engineering, automatic manufacturing system and so on due to its many advantages, such as larger hardness, higher strength and lower cost [1-4]. Especially, carbon steel is essential for the modern construction field which is usually made of holders, fasteners and so on [5-8]. However, there are a lot of cements, sands and concretes in the construction environment. The chloride ions, calcium ions and hydroxide ions in the harsh concrete environments are easy to produce electrochemical corrosion for carbon steel and shorten the service life of carbon steel. Therefore, it is very necessary to improve the corrosion resistance of carbon steel as a construction material. At present, it is reported that many chemical and physical surface treatments can

improve the corrosion resistance of carbon steel to meet the requirement of the construction field. For example, passivation treatment is an effective way to improve the corrosion resistance of carbon steel by immersion of the carbon steel in the nitric acid solution [9-12]. The passivation film produced on the surface of carbon steel by the passivation process has excellent corrosion resistance, but its thickness is thin, which is not conducive to working in a harsh environment for a long time. Some sols such as silica sol, titanium dioxide sol, etc. are reported that can be fabricated on the surface of carbon steel to improve corrosion resistance by the sol-gel method, but the adhesion force of sols is not good enough [13-15]. NiP electrodeposited coating is studied and verified as a kind of coating with better corrosion resistance. It is reported that appropriate phosphorus is beneficial to improve corrosion resistance [16-18]. Nevertheless, higher phosphorus in the alloy coating is bad for the improvement of corrosion resistance. Nano-SiC has the advantage of stable chemical properties, good wear resistance, excellent corrosion resistance and so on [19-20]. In this paper, Ni, NiP and NiP/SiC composite coatings were prepared on the surface of A105 carbon steel by electrodeposition technology, and the thickness, roughness, morphology, and corrosion resistance of the coatings were studied and analyzed. The corrosion mechanism of Ni/P and NiP/SiC composite coatings was revealed, which has a certain reference for improving the corrosion resistance of carbon steel.

2. EXPERIMENTAL

2.1 Chemical agents and materials

The A105 carbon steel is selected as the substrate to be electrodeposited Ni coating, NiP coating and NiP/SiC coating. The exposed area of the A105 carbon steel is 2 cm×2 cm while the pure platinum plate with a size of 3 cm×3 cm is the counter electrode. A saturated calomel electrode is used as the reference electrode. The substrate was immersed in the alkaline solution (15 g/L NaOH and 30 g/L Na_2CO_3) for 15 minutes at 60 ℃. After that, the substrate was put into the acid solution (10% HCl) for 2 minutes at 30 ℃ to remove rust. Finally, pure water was used to clean the substrate. The chemical agents used in the experiment are listed in Table 1 below.

Table 1. The composition of plating bath for Ni, NiP and NiP/SiC electrodeposition; All the chemical agents are analytically pure and the plating solution is 100 ml;

Chemical agent	Content(g/L)	Content(g/L)	Content(g/L)
	Ni coating	NiP coating	NiP/SiC coating
$NiSO_4·6H_2O$	30	30	30
$(NH4)_2C_6H_6O_7$	50	50	50
Na_2SO_4	30	30	30
NH_2CH_2COOH	10	10	10
H_3BO_3	30	30	30
NaH_2PO_2	-	10	10
Nano-SiC	-	-	2

According to Table 1, nickel sulfate and sodium hypophosphite in the plating solution offer nickel and phosphorus respectively for composite coating. Before the plating, ultrasonic oscillation is used to disperse the nano-SiC particles in the plating solution. Electrodeposition of Ni coating, NiP coating and NiP/SiC composite coating is all at the condition of 30 mA/cm^2 current density, 3600 s plating time, pH=3 and 60 ℃ temperature.

2.2 Performance testing

The electrochemical station (CHI660E) is used to analyze the chronoamperometry of Ni, NiP and NiP/SiC electrodeposition on the A105 substrate. The applied potential is selected as -1.0 V, -1.2 V and -1.4 V respectively for 300 s. Moreover, the corrosion resistance of coating in simulated concrete pore solution (saturated calcium hydroxide solution, 1 g/L NaOH, 3 g/L KOH and 3 g/L NaCl) is analyzed by potentiodynamic polarization curve. The potential is from -1.0 V to 0.5 V while the scan rate is set as 1 mV/s. Meanwhile, the 1 cm×1 cm A105 substrate is used as the cathode and the pure platinum plating with the size of 3 cm×3 cm is as the anode. The reference electrode is the saturated calomel electrode. The roughness and thickness of the coatings are tested by Klatencor P6 with 3D mode at the scan rate of 10 μm/s and 2 mg applied force. The surface morphology of the electrodeposited coatings is observed by scanning electron microscope S3400N at the condition of 15 kV accelerating voltage. The morphology of coatings after potentiodynamic polarization testing is analyzed by metallographic microscope MX63.

3. RESULTS AND DISCUSSION

3.1 Chronoamperometry curve of Ni, NiP and NiP/SiC electrodeposition

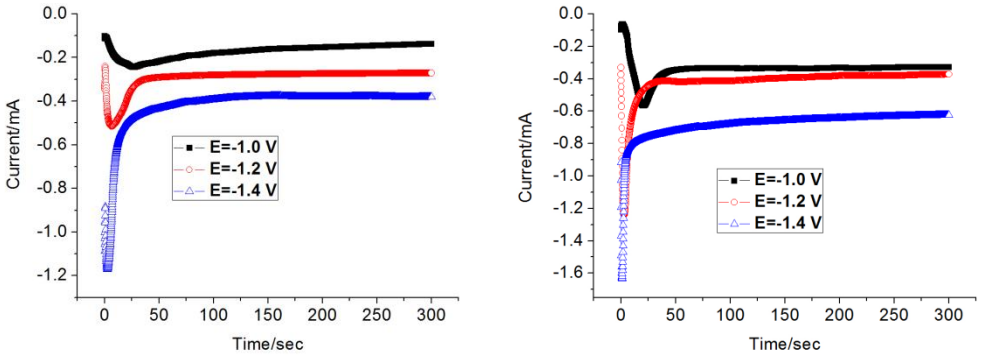

(a) Ni electrodeposition (b) NiP electrodeposition

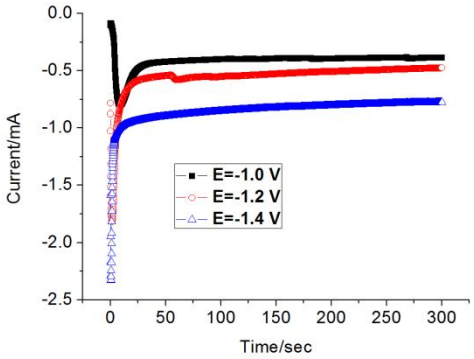

(c) NiP/SiC electrodeposition

Figure 1. Chronoamperometry curve of Ni, NiP and NiP/SiC electrodeposition on A105 substrate:(a) Ni electrodeposition from solution with 0.01 mol/L $NiSO_4$; (b) NiP electrodeposition from solution with 0.01 mol/L $NiSO_4$ and 0.01 mol/L NaH_2PO_2; (c) NiP/SiC electrodeposition from solution with 0.01 mol/L $NiSO_4$, 0.01 mol/L NaH_2PO_2 and 0.01 mol/L nano-SiC particles; The applied potential is -1.0 V, -1.2 V and -1.4 V respectively for 300 s at the temperature of 60 ℃;

Chronoamperometry curve of Ni, NiP and NiP/SiC electrodeposition at different potentials from -1.0 V to -1.4 V was investigated in Figure 1. Some people use quartz crystal microbalance and electrochemical station to study the cyclic voltammetry and chronoamperometry curve of nickel. They find that cathode current and deposition mass of nickel increase extremely when the potential ranges from -1.0 V to -1.5 V [21]. Moreover, the electrochemical behavior of NiP electrodeposition is studied by Ordine who discovers that the NiP electrodeposition is dominant when the potential is higher than -1.0 V [22]. In addition, some researchers also investigate the chronoamperometry curve of nickel alloys electrodeposition at the potential of -1.1 V, -1.2 V and -1.3 V [23]. Therefore, the potential of -1.0 V, -1.2 V and -1.4 V is applied to research the chronoamperometry curve. According to the chronoamperometry curve of Ni, NiP and NiP/SiC electrodeposition at the potential of -1.0 V, -1.2 V and -1.4 V, it is obvious that each curve shows a minimum and maximum value. In the early stage of electrodeposition, the cathode current decreases due to the charging of the double layer, and the minimum value appears. With the progress of electrodeposition, the metal ions in the solution obtain the electrons to be reduced to metal particles deposited on the surface of the cathode. A large number of metal particles deposited on the cathode surface increase the surface area, and the cathode current gradually increases to the maximum value. When the deposition process and the ion mass transfer process reach a balance, the cathode current tends to be stable. From Figure 1(a), the cathode current of Ni electrodeposition is stable at around -0.2 mA at the condition of -1.0 V. With the increase of potential from -1.0 V to -1.2 V, the cathode current of Ni electrodeposition increases from -0.2 mA to -0.4 mA.

$$Ni^{2+} + H_2O \Leftrightarrow (NiOH)^+ + H^+ \qquad (1)$$

$$(NiOH)^+ + 2e + H^+ \Leftrightarrow Ni + H_2O \qquad (2)$$

As can be seen from Equation (1) and Equation (2), the electrodeposition of nickel can be divided into two steps [24-25]. Nickel ions are hydrolyzed into $(NiOH)^+$ in the aqueous solution. After that, the $(NiOH)^+$ gets electrons to be reduced to nickel in acid environment. Regarding to Figure 1(b),

the cathode current of NiP electrodeposition is larger than that of NiP electrodeposition at the condition of same potential, indicating that sodium hypophosphate is involved in the electrochemical reaction process shown in Equation (3).

$$H_2PO_2^- + e^- \rightarrow P + 2OH^- \qquad (3)$$

Moreover, the chronoamperometry curve of NiP/SiC electrodeposition at the potential of -1.0 V, -1.2 V and -1.4 V can be seen in Figure 1(c). It is found that the cathode current of NiP/SiC electrodeposition is higher than that of Ni electrodeposition and NiP electrodeposition. The charge on the nano-SiC surface in an aqueous solution is generated by the decomposition of silanol. $[Si\text{-}OH_2]^+$ is generated by the reaction of silanol and hydrogen ions in an aqueous solution, which makes the surface of nano-SiC positively charged and migrates to the cathode surface, and is embedded in the alloy of Ni and NiP coating to form NiP/SiC composite coating.

3.2 Thickness and roughness of Ni, NiP and NiP/SiC coating

The thickness of Ni, NiP and NiP/SiC electrodeposited coating is shown in Figure 2 and Table 2. It can be seen that the average thickness of Ni, NiP and NiP/SiC coating is about 21.39 μm, 27.32 μm and 38.27 μm respectively. According to the previous analysis on the chronoamperometry curve of Ni, NiP and NiP/SiC electrodeposition, the cathode current of NiP/SiC electrodeposition is much higher than that of Ni and NiP electrodeposition at the same potential. Since nano-SiC particles are positively charged in an aqueous solution, which will migrate to the cathode surface and embed into Ni and NiP alloy coating during electrodeposition, increasing deposition rate and thickness. On the other hand, nano-SiC particles are easy to absorb nickel ions in an aqueous solution, which accelerates the migration of nickel ions to the cathode surface, leading to a further increase of deposition rate and thickness. Some scholars investigate the effect of SiC concentration on the thickness of the electrodeposited coating as well [26].

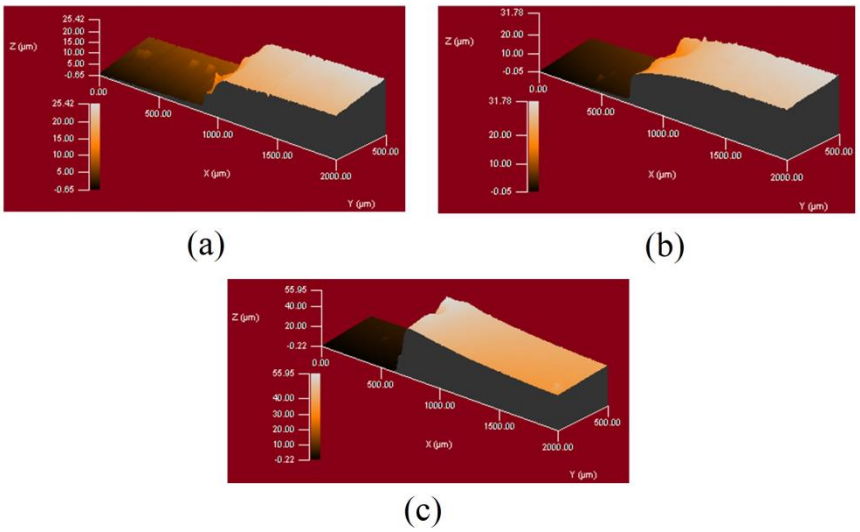

Figure 2. Thickness of Ni, NiP and NiP/SiC composite coating; The scan area is 2000 μm×500 μm with 10 μm/s scan rate; The applied force is 2 mg with sample rate 100 Hz;

Table 2. The average thickness of Ni, NiP and NiP/SiC composite coating; The scan area is 2000 μm×500 μm with 10 μm/s scan rate, 2 mg applied force and 100 Hz sample rate;

Samples	Minimum Thickness (μm)	Maximum Thickness (μm)	Average Thickness (μm)
Ni coating	19.38	22.42	21.39
NiP coating	25.12	28.78	27.32
NiP/SiC coating	37.49	41.95	38.27

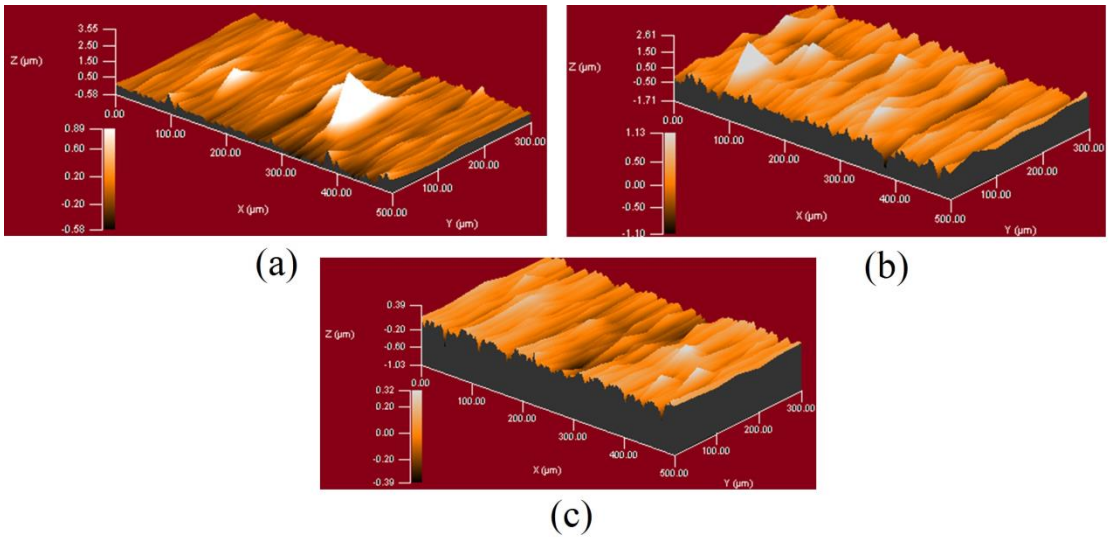

Figure 3. The roughness of Ni, NiP and NiP/SiC composite coating; The scan area is 500 μm×300 μm with 10 μm/s scan rate; The applied force is 2 mg with sample rate 100 Hz;

Surface roughness refers to the unevenness of small peaks and valleys on the coating surface. Contour arithmetic mean deviation Ra is selected as the surface roughness for electrodeposited coatings in the paper. According to Figure 3, the roughness of Ni, NiP and NiP/SiC is about 0.76 μm, 0.53 μm and 0.23 μm respectively. The roughness of the electrodeposited nickel coating is about 0.76 μm. It is reported that the electrodeposited nickel coating mainly exhibits granular or strip structure morphology, so the surface has certain ups and downs, and the roughness is large. The roughness of electrodeposited NiP alloy is lower than that of Ni alloy, which is mainly attributed to the precipitate of a large amount of phosphorus in the process of electrodeposition, which inhibits the growth of crystal nuclei and refines grains, thus reducing the roughness. The prepared NiP/SiC coating has the smallest roughness and the most compact and flat surface. In the electrodeposition process, the nano-SiC adsorbs nickel ions which migrate to the cathode surface under the action of the electric field, and the NiP/SiC composite coating is precipitated by discharge. The nano-SiC embedded in NiP alloy can induce lattice distortion, further refine the grains, and greatly reduce the roughness [27-28].

3.3 Surface morphology and corrosion resistance of Ni, NiP and NiP/SiC coating

The surface morphology of different coatings including Ni, NiP and NiP/SiC is presented in Figure 4. As can be seen, different coatings show diverse surface morphology. The surface of nickel coating shows a typical combination of strip and granular morphology with rough surface and different particle sizes. With the addition of sodium hypophosphite in the bath, the surface of the NiP coating mainly exhibits typical nodular particle morphology. Compared with nickel coating, the surface particles of NiP coating are smaller, uniform and compact. The main reason is that phosphorus can inhibit nucleation and refine grains during electrodeposition. Similar surface morphology of NiP electrodeposition is reported by Lelevic as a review paper published in the journal of surface and coatings technology [29].

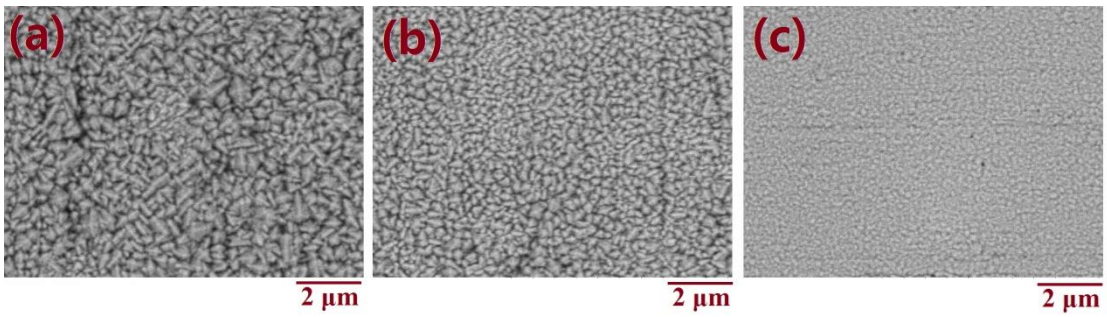

Figure 4. Surface morphology of Ni, NiP and NiP/SiC composite coating; (a) Ni electrodeposited coating; (b) NiP electrodeposited coating; (c) NiP/SiC electrodeposited composite coating; The accelerating voltage is 15 kV and the working distance is 10 mm;

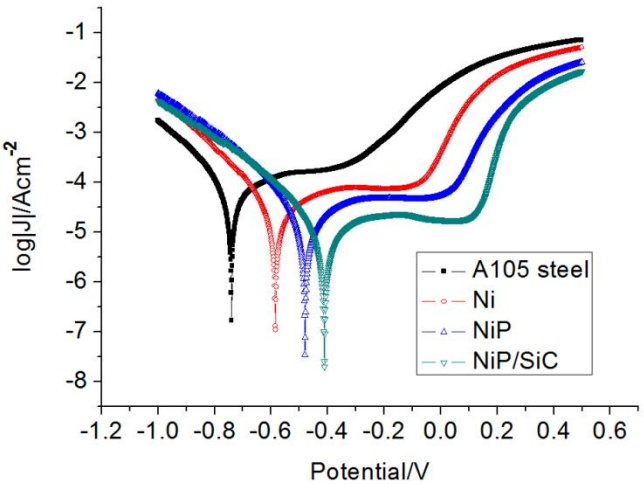

Figure 5. Potentiodynamic polarization curve of different electrodeposited coatings in simulated concrete pore solution; (a) A105 steel; (b) Ni coating; (c) NiP coating; (d) NiP/SiC coating; The potential is from -1.0 V to 0.5 V while the scan rate is set as 1 mV/s; The 1 cm×1 cm A105 substrate is used as the cathode and the pure platinum plating with size of 3 cm×3 cm is as the anode; The reference electrode is the saturated calomel electrode;

Table 3. Corrosion potential and corrosion current density of different coatings in simulated concrete pore solution;

Samples	E_{corr} (V)	J_{corr} (μA/cm^2)
A105 steel	-0.747	56.23
Ni coating	-0.584	26.74
NiP coating	-0.476	12.59
NiP/SiC coating	-0.417	7.94

The surface morphology of NiP/SiC composite coating is shown in Figure 4(b). It can be found that the surface of NiP/SiC composite coating is composed of uniform and compact particles. Compared with Ni and NiP coatings, NiP/SiC composite coating has the smallest surface particle size and the lowest roughness. Nano-SiC can absorb nickel ions in the bath and embed into NiP coating, inducing lattice distortion, which greatly reduces the size of surface particles and improves the compactness. The effect of SiC on the surface morphology of nickel alloys has been researched by some people [30-31].

The potentiodynamic polarization curves of different electrodeposited coatings are presented in Figure 5. The E_{corr} and J_{corr} are calculated and listed in Table 3. According to the data of Figure 5 and Table 3, the corrosion potential and corrosion current density of A105 steel substrate is about -0.74 V and 56.23 μA/cm^2 respectively. In addition, the corrosion current density of the Ni coating and NiP coating is around 26.74 μA/cm^2 and 12.59 μA/cm^2 which are both lower than that of A105 steel substrate, indicating that the corrosion resistance of Ni coating and NiP coating is better than A105 steel. The NiP/SiC composite coating has the lowest corrosion current density and the most positive corrosion potential, indicating the best corrosion resistance performance. The simulated concrete pore solution is an alkaline solution, and the nickel coating is easy to produce corrosion products (nickel hydroxide) in the alkaline condition during the corrosion process, which inhibits the corrosion process to a certain extent. In the process of electrochemical corrosion, the surface of NiP coating is enriched with phosphorus element due to the continuous dissolution of nickel, which can further inhibit electrochemical corrosion. The higher impedance of nano-SiC particles in NiP/SiC coating can further disperse the corrosion current, so the corrosion resistance is greatly improved. Many scholars also point out that the SiC particles in the plating solution can effectively improve the corrosion resistance of electrodeposited coating [32-33].

The surface morphology of different samples after potentiodynamic polarization testing is shown in Figure 6. It can be seen from Figure 6(a) that the corrosion resistance of A105 substrate is poor in the alkaline simulated concrete pore solution. After potentiodynamic polarization testing, the surface of A105 substrate shows many larger corrosion holes. Compared with A105 substrate, the size and number of corrosion holes on Ni coating and NiP coating surface are smaller and less. According to the potentiodynamic polarization curve data, the NiP/SiC composite coating has the smallest corrosion current density, and the number of corrosion holes on its surface is also the smallest.

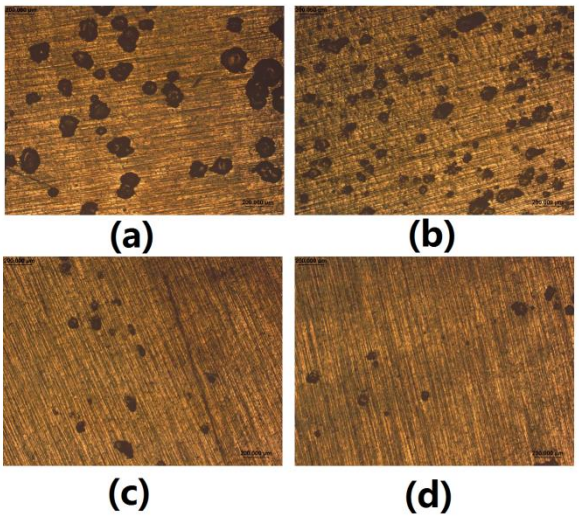

Figure 6. The surface morphology of Ni, NiP and NiP/SiC coating after potentiodynamic polarization testing; (a) A105 steel; (b) Ni coating; (c) NiP coating; (d) NiP/SiC coating; Magnification is 100 times and light source is 12V, 50W halogen lamp;

4. CONCLUSIONS

The Ni coating, NiP coating and NiP/SiC composite coating are electrodeposited on the A105 steel as a construction material to investigate its corrosion behavior in the simulated concrete pore solution. Moreover, chronoamperometry curves, thickness, roughness and surface morphology of different coatings are also investigated.

(1) It is found that the cathode current of NiP/SiC electrodeposition is higher than that of Ni electrodeposition and NiP electrodeposition. The surface of nano-SiC is positively charged in the plating solution and migrates to the cathode surface, which is embedded in the alloy of Ni and NiP coating to form NiP/SiC composite coating. The average thickness of Ni, NiP and NiP/SiC coating is about 21.39 μm, 27.32 μm and 38.27 μm respectively.

(2) The prepared NiP/SiC coating has the smallest roughness and the most compact and flat surface. The nano-SiC embedded in NiP alloy can induce lattice distortion, further refine the grains, and greatly reduce the roughness. According to the data of the potentiodynamic polarization curve, the NiP/SiC composite coating possesses the best corrosion resistance with the smallest corrosion current density, and the number of corrosion holes on its surface is also the smallest.

References

1. J. K. Ren, D. S. Mao, Y. Gao, J. Chen and Z. Y. Liu, Mater. *Sci. Eng., A,* 827 (2021) 141959.
2. X. F. Cao, Y. Z. Zhang, W. Hu, H. A. Zheng, Y. Dan, J. Hu and Z. Chen, Mater. Des., 211 (2021) 110169.
3. L. Keshav, V. S. Teja and J. Vairamuthu, *Mater. Today:. Proc.*, 33 (2020) 4498.
4. G. Jena, R. P. George and J. Philip, *Prog. Org. Coat.*, 161 (2021) 106462.
5. M. Moradi and M. Rezaei, *Constr. Build. Mater.*, 317 (2022) 126136.
6. X. X. Song, K. Y. Wang, L. Zhou, Y. J. Chen, K. X. Ren, J. Y. Wang and C. Zhang, *Eng. Fail. Anal.*,

134 (2022) 105987.
7. K. Srinivasan, J. S. Sudarsan and S. Nithiyanantham, *Case Stud. Constr. Mater.*, 15 (2021) e00716.
8. S. I. Evans, J. Wang, J. Qin, Y. P. He, P. Shepherd and J. L. Ding, *Struct.*, 44 (2022) 1506.
9. T. Wu, X. Y. Lu, Z. Chen, X. G. Feng, Y. J. Zhang, X. F. Chen and N. Zhuang, *Corros. Sci.*, 198 (2022) 110102.
10. Z. J. Song, Y. J. Zhang, L. Liu, Q. Pu, L. H. Jiang, H. Q. Chu, Y. Y. Luo, Q. Y. Liu and H. C. Cai, *Constr. Build. Mater.*, 274 (2021) 121779.
11. S. Suresh, C. Palogi, S. Bera and R. Srinivasan, *Thin Solid Films*, 721 (2021) 138550.
12. G. C. Rosado and M. A. P. Canul, *Corros. Sci.*, 153 (2019) 19.
13. E. P. Grishina, N. O. Kudryakova and L. M. Ramenskaya, *Thin Solid Films*, 746 (2022) 139125.
14. A. S. Vega, C. A. Saenz, L. A. Odell, F. Brusciotti, A. Somers and M. Forsyth, *Appl. Surf. Sci.*, 561 (2021) 149881.
15. L. X. Bach, D. V. Thuan, V. T. H. Thu, T. B. Phan, N. S. H. Vu and N. D. Nam, J. *Mater. Res. Technol.*, 8 (2019) 6400.
16. K. Grajewska and M. Lieder, *Diamond Relat. Mater.*, 118 (2021) 108533.
17. L. H. Guo, Q. Huang, C. Zhang, J. Wang, G. P. Shen, C. L. Ban and L. X. Guo, *Corros. Sci.*, 178 (2021) 108960.
18. M. Z. Wang, R. Ma, A. Du, S. H. Hu, M. Muhammad, X. M. Cao, Y. Z. Fan, X. Zhao and J. J. Wu, *Mater. Chem. Phys.*, 250 (2020) 123056.
19. J. Q. Wu, Z. Li, Y. Luo, Y. Li, Z. L. Gao, Y. B. Zhao, C. W. Wu, Y. X. Liao and M. Jin, *Tribol. Int.*, 175 (2022) 107865.
20. M. A. Hernandez, K. D. Bakoglidis, P. J. Withers and P. Xiao, *Wear*, 456 (2020) 203399.
21. Y. D. Yu, L. X. Sun, H. L. Ge, G. Y. Wei and L. Jiang, *Int. J. Electrochem. Sci*., 12 (2017) 485.
22. A. P. Ordine, S. L. Diaz, I. C. P. Margarit, O. E. Barcia and O. R. Mattos, *Electrochim. Acta*, 51 (2006) 1480.
23. M. Ebadi, W. J. Basirun, Y. Alias, M. R. Mahmoudian and S. Y. Leng, *Mater. Charact.*, 66 (2012) 46.
24. P. M. Ming, W. X. Lv, Y. J. Li, J. Y. Shang and J. T. Wang, *Electrochim. Acta*, 120 (2014) 6.
25. T. Borkar and S. P. Harimkar, *Surf. Coat. Technol.*, 205 (2011) 4124.
26. R. J. Ji, K. Han, H. Jin, X. P. Li, Y. H. Liu, S. G. Liu, T. C. Dong, B. P. Cai and W. H. Cheng, *J. Manuf. Processes*, 57 (2020) 787.
27. Y. H. Chen and L. Gou, *Diamond Relat. Mater.*, 129 (2022) 109377.
28. O. S. A. Rahman, N. P. Wasekar, G. Sundararajan and A. K. Keshri, *Mater. Charact.*, 116 (2016) 1.
29. A. Lelevic and F. C. Walsh, *Surf. Coat. Technol.*, 378 (2019) 124803.
30. J. A. Calderon, J. E. Henao and M. A. Gomez, *Electrochim. Acta*, 124 (2014) 190.
31. M. A. Samani, B. Ghasemi and M. Khodaei, *Thin Solid Films*, 736 (2021) 138914.
32. H. B. Zhang, J. D. Wang, S. X. Chen, H. Wang, Y. He and C. Y. Ma, *Ceram. Int.*, 47 (2021) 9437.
33. W. Jiang, L. Shen, M. Y. Xu, Z. W. Wang and Z. J. Tian, *J. Alloys Compd.*, 791 (2019) 847.